

Numerical study of linear and circular model DNA chains confined in a slit: metric and topological properties

Cristian Micheletti*

SISSA - Scuola Internazionale Superiore di Studi Avanzati and CNR-IOM Democritos, Via Bonomea 265, 34136 Trieste (Italy)

Enzo Orlandini†

*Dipartimento di Fisica e Astronomia and Sezione INFN,
Università di Padova, Via Marzolo 8, 35131 Padova (Italy)*

(Dated: March 1, 2022)

Advanced Monte Carlo simulations are used to study the effect of nano-slit confinement on metric and topological properties of model DNA chains. We consider both linear and circularised chains with contour lengths in the 1.2–4.8 μm range and slits widths spanning continuously the 50–1250nm range. The metric scaling predicted by de Gennes’ blob model is shown to hold for both linear and circularised DNA up to the strongest levels of confinement. More notably, the topological properties of the circularised DNA molecules have two major differences compared to three-dimensional confinement. First, the overall knotting probability is non-monotonic for increasing confinement and can be largely enhanced or suppressed compared to the bulk case by simply varying the slit width. Secondly, the knot population consists of knots that are far simpler than for three-dimensional confinement. The results suggest that nano-slits could be used in nano-fluidic setups to produce DNA rings having simple topologies (including the unknot) or to separate heterogeneous ensembles of DNA rings by knot type.

I. INTRODUCTION

Nano-devices are increasingly used to investigate the impact of spatial restraints on the statics and dynamics of polymers and biopolymers. DNA is ideally suited for such studies both for its applicative potential (nano-confinement can be used to sort, sieve and sequence DNA [1–4]) and because its elastic properties can be exploited to elucidate issues of primary interest in polymer science [5–11]. In fact, the width of presently-available confining nano-devices (a channel, a slit, a pit etc.) can be set to compete with one or more of the characteristic lengths of a DNA molecule and hence allow for probing different physical regimes [8, 11–18].

A classic example is offered by the one-dimensional (channel) confinement of linear DNA molecules whose elongation follows two different scaling laws, named after de Gennes [12] and Odijk [19], according to whether the channel width is larger or smaller than l_p [20]. A second notable instance is offered by DNA molecules confined in three-dimensions, as inside a viral capsid. In the latter case, the interplay of the genome length and capsid size, can profoundly affect the entanglement of the packaged DNA [21–24]. Both aspects are aptly revealed by the abundance and complexity of knots that are trapped in DNA filaments that circularise inside viral capsids [11, 17, 25–30].

Compared to the above one- and three-dimensional cases, two-dimensional polymer confinement is much less characterised both for the metric and topological properties. To the best of our knowledge there exist only

a limited number of experimental and numerical studies of the size and shape of DNA molecules in nano-slits [8, 18, 31–33]. These seminal studies have addressed the interesting issue of whether multiple scaling regimes exist in *linear* DNA filaments inside slits. It appears that the same question has not been posed for circularised DNA molecules where, unlike the linear case, entanglement is trapped in the form of topological constraints (knots) which affect the physical behaviour and biological functionality [34–41]. The impact of slit confinement on the topology of circularised polymers has been previously addressed by early simulations of lattice polymer models [42] so that its implications for slit-confined DNA are virtually unexplored.

As a step towards clarifying the above-mentioned aspects we carry out a systematic numerical study of linear and circularised chains in nano-slits whose salient physical properties, namely the thickness and bending rigidity are set to match those of dsDNA. Specifically we use advanced Monte Carlo techniques to characterize the shape, orientation and entanglement of linear and circularised chains of contour lengths in the 1.20–4.8 μm range and confined in nano-slits of width from 50 to 1250 nm.

The computational scheme is first used to characterize the metric scaling by varying independently the chain contour length and the slit width. The metric scaling predicted by de Gennes’ blob model is found to hold, up to the strongest levels of confinement, for both linear and circular chains.

Next, we show that two-dimensional confinement affects the ring topology in a qualitatively different way from three-dimensional confinement. In fact, for increasing three-dimensional confinement both the incidence and complexity of knots grows monotonically [23, 24]. In the two-dimensional case, instead,

*Electronic address: michelet@sissa.it

†Electronic address: orlandini@pd.infn.it

the knotting probability is non-monotonic and the knot spectrum mostly consist of the simplest knot types. The fraction of knotted molecules is maximum, and exceeds by several times the bulk (unconstrained) value, when the slit width is a fraction of the average extension of the unconstrained chains. A reduction of the width below this value, causes the knotting probability to decrease rapidly.

This fact offers the opportunity to use the set-up of two-dimensional confinement in nano-slits as an effective method to produce DNA rings with an *a priori* control on their topology and that can be tuned to yield a proportion of knotted molecules that is much higher or much lower than the bulk one. In addition, the sensitive dependence of the conformational entropy of knotted molecules with different topology on the size of the confining region, suggests that width-modulated slits could be profitably used in nano-fluidic setups to sort circular DNAs by knot type.

II. METHODS

A. The model

For this study, dsDNA is modelled as a semi-flexible chain of cylinders. This coarse-grained model captures appropriately the metric and topological properties of DNA both when it is unconstrained [43, 44] and when it is packed at moderate densities, that is for interstrand separations larger than $\approx 5\text{nm}$ [45]. In such conditions, which are met in our study, dehydration effects and cholesteric interactions can be neglected [11, 17, 28, 46, 47]. It is further assumed that DNA is in a concentrated buffer of monovalent counterions so that the screened electrostatic repulsion can also be neglected. The cylinder diameter is accordingly set equal to the dsDNA hydration diameter, $d = 2.5\text{nm}$. Notice that no potential energy term is introduced to account for the DNA torsional rigidity. Its interplay with bending rigidity can, *a priori* impact the relevant conformational space of densely packed DNA, as argued in ref. [48] for closed DNA chains. However, recent independent simulations of three-dimensionally confined DNA with free ends have shown that torsional effects are negligible even at packing densities higher than considered here [49]. We shall therefore work under the hypothesis that the slit-confined DNA chains are torsionally relaxed both in the linear and in the circularised form. For the latter case it is assumed that DNA circularization occurs via non-covalent annealing of the DNA sticky ends so that all torsional stress can still be released.

We consider open and closed chains of contour length equal to L_c ranging from $1.2\ \mu\text{m}$ to $4.8\ \mu\text{m}$ and describe them as chains of cylinders with $N = 120 \dots 480$ vertices, respectively, as shown in Table I. This discretization level corresponds to a long axis of the cylinder, b ,

approximately equal to 10nm which is a fraction of the DNA persistence length, $l_p = 50\text{nm}$.

N	bp	L_c [nm]	Linear R_g^0 [nm]	Circular R_g^0 [nm]
120	3534	1201	128 ± 3	94 ± 3
240	7068	2403	190 ± 5	136 ± 5
320	9426	3204	222 ± 6	159 ± 6
360	10602	3604	236 ± 6	169 ± 6
400	11782	4006	251 ± 6	179 ± 6
480	14136	4806	276 ± 7	198 ± 7

TABLE I: Parameters of the simulated linear and circular DNA molecules: N is number of cylinders of the model chains, bp is the total number of base-pairs and L_c is the corresponding contour length. The last two columns provide the bulk values of the root mean square radius of gyration, R_g^0 of the linear and circular chains.

The potential energy of a chain configuration, Γ , consists of two terms, $E_\Gamma = E_{excl-vol}(\Gamma) + E_b(\Gamma)$. The first term is the excluded volume interaction which enforces the chain self-avoidance. $E_{excl-vol}$ is set equal to “infinity” if two non-consecutive cylinders overlap, otherwise is set equal to zero. The second term, E_b is the bending potential energy:

$$E_b = -K_b T \frac{l_p}{b} \sum_i \vec{t}_i \cdot \vec{t}_{i+1} \quad (1)$$

where \vec{t}_i is the orientation of the axis of the i th cylinder and the temperature T is set to 300K . For linear chains, i runs from 1 to N . For circular ones, instead, i runs from 1 to $N + 1$ with the proviso that $\vec{t}_{N+1} \equiv \vec{t}_1$.

DNA confinement in nano-slit is modelled by setting an upper bound, D , to the calliper size of the chains along one direction, conventionally taken as the z axis of the system Cartesian coordinate, see Fig. 1. Because the z direction is perpendicular to the two impenetrable planes delimiting the slit, all observables measured along this direction will be indicated with the \perp subscript, while those measured parallel to the slit plane will be denoted with the \parallel subscript.

B. Advanced sampling techniques

An advanced Monte Carlo sampling technique is used to compute the equilibrium metric and topological observables of open and closed chains subject to slit confinement. The technique is described in detail in a recent review article [11] and therefore we shall describe it only concisely.

The method consists of using a standard set of crankshaft and pivot moves to evolve the chains but the canonical weights used for the Metropolis acceptance criterion are generalised to ensure that configurations are sampled according to the following (non-normalised) statistical weight:

$$\exp \left\{ -\frac{E_{excl-vol}(\Gamma) + E_b(\Gamma) - \mu \Delta_\perp(\Gamma)}{K_b T} \right\}. \quad (2)$$

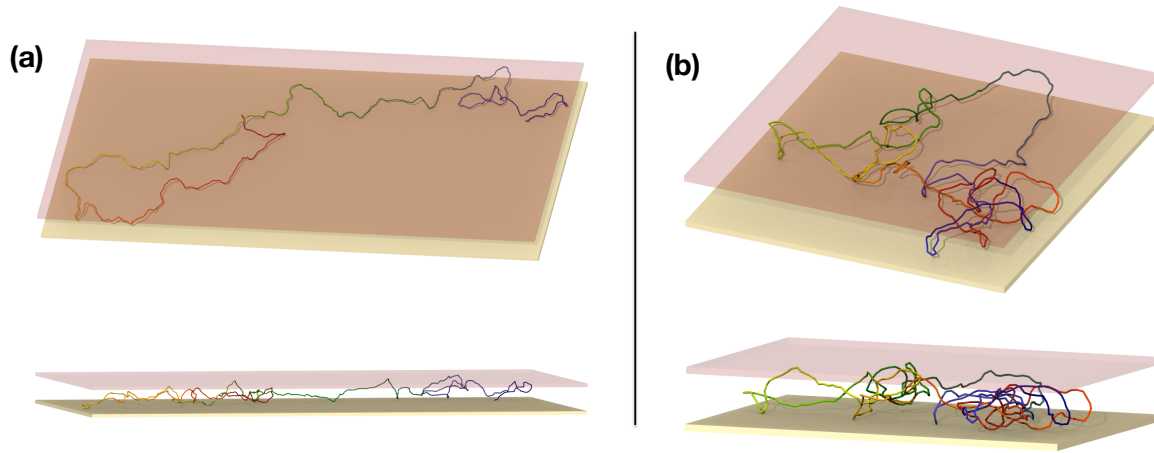


FIG. 1: Two views of a confined semiflexible linear (panel a) and circular (panel b) chains of 480 cylinders, equivalent to a contour length $L_c = 0.48\mu\text{m}$. In both cases the slit width is $D = 70\text{nm}$.

where $\Delta_{\perp}(\Gamma)$, is the configuration calliper size measured along the confining, z direction. The non-negative quantity μ can be viewed as an anisotropic pressure promoting the confinement along z . In fact, by increasing μ one can reduce the average calliper size of the generated configurations. By using a multiple Markov chain scheme, consisting of several parallel Monte Carlo simulations each at a different value of μ [23, 50], it is possible to sample very effectively configurations covering a wide range of calliper size, $\Delta_{\perp}(\Gamma)$. Finally, a thermodynamic reweighting technique analogous to the one used in ref.[23] is used to combine the observables computed for configurations generated at various values of μ . This procedure gives an estimate of the equilibrium properties of chains that can be accommodated inside slits of width, D , in the 50nm - 1250nm range.

C. Metric properties

The average size, shape anisotropy, and orientation of a given ring are characterized by means of the eigenvalues and eigenvectors of its gyration tensor, \mathbf{Q} . The entries of this 3×3 symmetric matrix are given by:

$$Q_{\alpha,\beta} = \frac{1}{N} \sum_{i=1}^N (\mathbf{r}_{i,\alpha} - \bar{\mathbf{r}}_{\alpha})(\mathbf{r}_{i,\beta} - \bar{\mathbf{r}}_{\beta}), \quad (3)$$

where \mathbf{r}_i is the position of the i th vertex of the chain, α and β run over the three Cartesian components and $\bar{\mathbf{r}} = \frac{1}{N} \sum_i \mathbf{r}_i$ is the average vertex position in the chain. The non-negative eigenvalues of \mathbf{Q} , ranked for decreasing magnitude, are indicated as Λ_1 , Λ_2 and Λ_3 and their associated (normalised) eigenvectors are indicated as \vec{e}_1 , \vec{e}_2 and \vec{e}_3 .

The sum of the eigenvalues provides the square radius of gyration of the chain:

$$R_g^2 = \Lambda_1 + \Lambda_2 + \Lambda_3, \quad (4)$$

while the adimensional ratios Λ_1/Λ_3 and Λ_2/Λ_3 are used to characterize the chain shape anisotropy.

The chain orientation inside the slit is conveniently described by the angle α formed by each principal gyration axis and the slit plane:

$$\cos \alpha_i = \sqrt{1 - |\vec{e}_i \cdot \hat{\mathbf{z}}|^2} \quad (5)$$

where $\hat{\mathbf{z}}$ is the unit vector in the z direction.

To parallel the quantities that are customarily measured in nano-slit experiments, for each chain configuration we compute its mean square size projected in and out of the slit plane which are, respectively:

$$R_{\parallel}^2 = \sum_{i=1,2,3} \Lambda_i \cos^2 \alpha_i, \quad (6)$$

$$R_{\perp}^2 = R_g^2 - R_{\parallel}^2 = \sum_{i=1,2,3} \Lambda_i (1 - \cos^2 \alpha_i). \quad (7)$$

D. Scaling properties and the deGennes regime

The de Gennes' blob theory provides a powerful reference framework for characterizing spatially constrained chains [12]. The theory, originally formulated to improve on standard mean-field theories for semidilute polymer solutions and [51, 52], has proved useful to understand the behaviour of polymers confined in regions with transverse size larger than the molecule's persistence length.

When such condition is met, the theory of de Gennes proposes to describe the self-avoiding chain, formed by N monomers of size b , as a sequence of "blobs", with each blob consisting of g monomers and having linear size about equal to the slit width, D , see Fig. 2. Within each blob, the chain does not experience the confining constraints and hence it behaves as an unconstrained self-avoiding walk: $D \sim g^{\nu_{3D}}$, where $\nu_{3D} \sim 0.588$

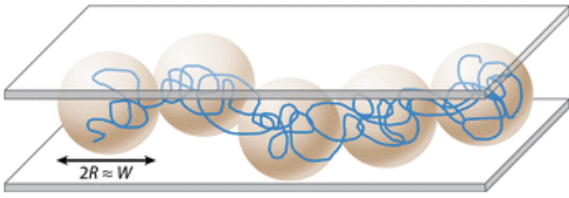


FIG. 2: Pictorial representation of a confined polymer as a string of DeGennes' blobs

is the three-dimensional self-avoiding walk scaling exponent [53]. At the same time, the string of blobs can be viewed as being a two-dimensional self-avoiding walk, with the blobs being the effective monomeric units of the walk. Accordingly, the in-plane size of the chain expectedly scales as $R_{||} \sim (N/g)^{\nu_{2D}} D$ where $\nu_{2D} = 3/4$ is the self-avoiding exponent in two dimensions.

This relationship can be recasted as $R_{||} \sim (N/g)^{\nu_{2D}} D \sim N^{\nu_{2D}} D^{-\nu_{2D}/\nu_{3D}} D$ or, equivalently,

$$\frac{R_{||}}{R_g^0} \sim \left(\frac{D}{R_g^0}\right)^{1-\nu_{2D}/\nu_{3D}} \sim \left(\frac{D}{R_g^0}\right)^{-0.276}, \quad (8)$$

where we have exploited the proportionality of R_g^0 and $R_{||}^0$ which are respectively the root mean square values of the radius of gyration and the in-plane projected size of unconstrained chains. It is worth pointing out that the prefactor entering the scaling relationship of eq. 8 changes according to whether the blobs are isotropic or not [13, 20]. This condition depends, in turn, on whether the slit width D is larger or smaller than l_p^2/d . For our case, the latter quantity is equal to $1\mu\text{m}$ and therefore is always larger than the widths of the slits considered. The blobs are therefore expected to be anisotropic (extended de Gennes regime) [20].

E. Topological properties

The characterization of the entanglement of circular configurations is completed by establishing their knotted state. It should be noted, in fact, that the crankshaft moves employed for the MC evolution preserve the ring connectivity but not necessarily its topology [54]. In fact, even if the initial and final state of a crankshaft move are self-avoiding, the virtual crankshaft movement that bridges them can entail several bond crossings and hence can change the ring knotted state.

The topology of a ring is established using the same methodology of ref. [23, 45] which is articulated over the following steps. First, the ring geometry is simplified by topology preserving moves [11, 23, 55, 56]. These moves consist of ring deformations involving no bond crossing and promote the collinearity of triplets of ring vertices that are nearby in sequence. After the chain simplification, a two-dimensional projection of

the resulting configuration is next taken, encoded as a digital Dowker code, simplified algebraically and finally compared against a lookup table of prime knots with up to 16 crossings. If a match is found for all the prime component of a knot, then the ring knotted topology is unambiguously established otherwise it is labelled as “unknown”.

Notice that the “unknown” states may correspond to complicated knots with prime components having more than 16 crossings, or may be a simple knot that could not be simplified enough to positively identify it.

Further insights on the interplay between the topological properties of circular DNAs and the degree of confinement may be obtained by considering the average length of the knotted region in the ring. Locating the knotted portions in closed chains is a challenging problem, that presents the same conceptual difficulties as establishing the knotted state of a geometrically-entangled open chain [11, 54]. Although the application of topological concepts to open chains is *a priori* ambiguous, it has been recently verified that very different methods for locating knots in linear chains yield remarkably consistent results [57]. Among them we mention those based on the statistical closure scheme [58] and the minimally-interfering one [57] which is used here for its robustness and numerical efficiency.

III. LINEAR DNA IN NANO-SLITS

A. Effect of confinement on chain orientation and shape

The effect of slit confinement on the chain orientation is illustrated in Fig. 3a.

The data reflect the in-plane and out-of-plane orientations, see eq. 5, of the three axes of inertia of open chains of contour length, $L_c = 3604$ nm. The bulk root mean square radius of gyration of these chains is $R_g^0 = 236$ nm (see Table I) and its location in the plots of Fig. 3 is depicted by the vertical dot-dashed line. For slit widths much larger than the chain bulk size the three mean square cosines are all close to the value $1/3$, as expected in case of isotropic orientation of the chain in space.

The orientation of the longest axis of inertia begins to be noticeably non-isotropic when the slit width is about 700nm, which exceeds three times the bulk radius of gyration. This is consistent with the strong shape anisotropy of unconstrained chains ($\Lambda_1/\Lambda_3 = 13.8$ and $\Lambda_2/\Lambda_3 = 3.05$) which implies that the longest axis of gyration cannot be freely-accommodated inside the slit already when the width D is several times larger than R_g^0 . The second longest axis of gyration is oriented isotropically, and maintains its bulk value, down to slit widths $D \approx 2R_g^0 = 472\text{nm}$ (shown in the panels of Fig. 3 as a dashed vertical line). The value of Λ_2 reduces appreciably when D is decreased down to about R_g^0 and remains approximately constant for smaller slit

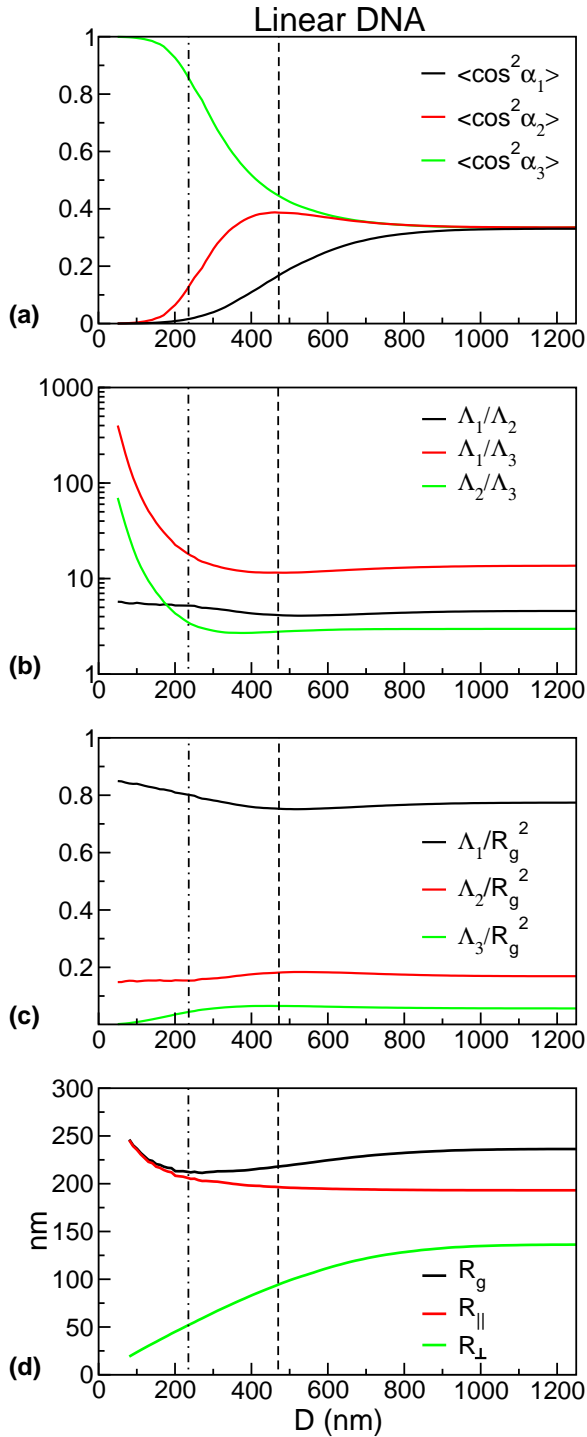


FIG. 3: Metric properties of a linear chain $L_c = 3604$ nm inside a slit of width D . The orientation, shape and size of the gyration ellipsoid of the confined chain are shown in panels (a–c). The root mean square values of the chain radius of gyration, and its in- and out-of-plane projections are shown in panel (d). The range and scale of the x axis (representing the slit width, D) is common to all panels. The two vertical lines mark the reference slit widths R_g^0 (dot-dashed) and $2R_g^0$ (dashed).

widths. Analogous properties are found for the other chain lengths considered in this study.

For $D < R_g^0$, both the first and the second axes of inertia are mostly confined in the slit plane, while the third is oriented perpendicularly to it.

The progressive in-plane orientation of the two principal axes of inertia is paralleled by the flattening of the chain in the slit plane, see Fig. 3b. From Fig. 3c it is noticed that for $D < 2R_g^0$ the progressive in-plane orientation of the second axis of inertia is accompanied by a decrease of its eigenvalue Λ_2 to a limiting value that is smaller than in the unconstrained, bulk case. The opposite is true for Λ_1 . As a result, strongly confined open chains tend to have an elongated shape, as in the example of Fig. 1a.

The adimensional data in Fig. 3b,c compares favourably with available numerical and experimental results for the limiting cases of no- and strong two-dimensional confinement. In particular, Haber et al. [59] report the aspect ratios $\sqrt{\Lambda_1/\Lambda_3} = 4.1$ and $\sqrt{\Lambda_1/\Lambda_2} = 2.3$ for *fully-flexible* unconstrained polymers, which are close to the corresponding values 3.7 and 2.1 found here. Finally, Maier *et al.*, in their study of λ -phage DNA adsorbed on a flat bilayer lipid membrane [60], found $\Lambda_1/R_g^2 = 0.84$ and $\Lambda_2/R_g^2 = 0.14$ which is in accord with the values $\Lambda_1/R_g^2 = 0.84 \pm 0.02$ and $\Lambda_2/R_g^2 = 0.148 \pm 0.008$ found here for the strongest two-dimensional confinement.

B. Effect of confinement on chain size

The global, in-plane and transverse size of the chain at various levels of confinement are shown in Fig. 3d.

The transverse size, R_{\perp} and the parallel one, $R_{||}$, have opposite monotonic dependence on D which result in a non-monotonic behaviour of R_g as a function of D . From Fig. 3d, it is seen that R_g is minimum for D about equal to the bulk radius of gyration of the chain, R_g^0 . This property is found consistently across chains of all considered lengths, as shown in Fig. 4a.

To test the validity of the de Gennes' blob regime we analyzed the D dependence of $R_{||}$. The result is shown in Fig. 4b which reveals a remarkable collapse of data points from curves of lengths L_c between $2.4\mu\text{m}$ and $4.8\mu\text{m}$. As shown in the figure, for high confinement $R_{||}$ has a power law dependence on D , with exponent equal to -0.27 ± 0.05 . This exponent, estimated by fitting the most asymptotic data i.e. $L_c \geq 3604$ nm, is well compatible with the -0.276 value predicted by the de Gennes' theory. Notice that, at all considered lengths no deviation from the de Gennes' theory is observed, consistently with the recent experiments of Doyle et al. [18] on longer DNA filaments.

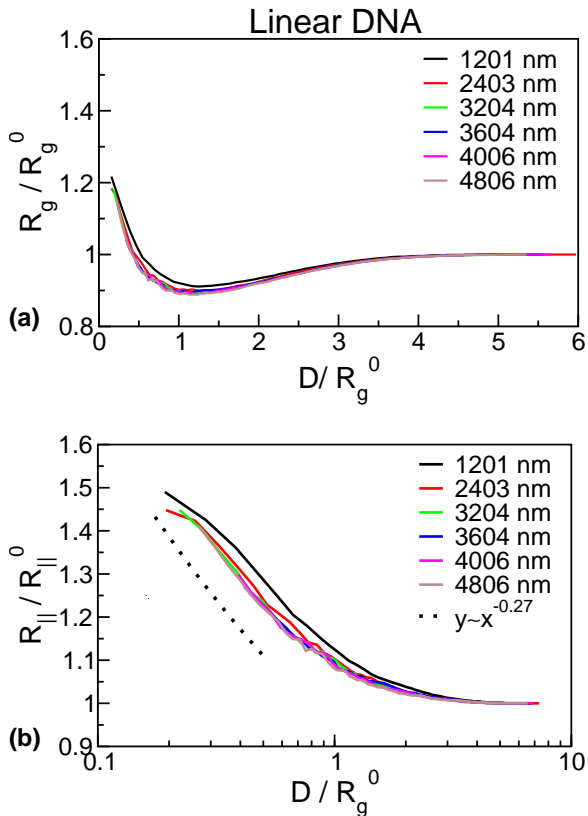


FIG. 4: (a) The minimum three-dimensional size of the chain is achieved when the slit width is about equal to the average radius of gyration of the unconstrained chain. (b) Below such slit width the relationship between the average in-plane size, R_{\parallel} , chain contour length, N , and slit width, D , is well accounted for by the DeGennes blob theory.

IV. CIRCULAR DNA IN NANO-SLITS

We consider DNA rings with the same contour length as the previously-discussed open chains, see Table I, and for the same range of confining slit widths. The properties of rings are first characterised at the metric level and then at the topological one. We shall particularly focus on the type, abundance and size of the various knots that are trapped in confined model DNA molecules that are circularized in equilibrium. These aspects are known to affect significantly the static and dynamics of polymers both in dilute [61, 62] and dense solutions [63] or tightly packed in small volumes [17, 24, 25, 27, 28, 57] or pulled through narrow channels [27, 28] and are hence expected to be important for two-dimensional confinement too.

A. Effect of confinement on ring orientation and size

The dependence of a ring size and orientation on the confining slit width is illustrated in Fig. 5. The data pertains to rings of length $L_c = 3604$ nm and therefore

can be directly compared with those in Fig. 3 for an equally-long open chain.

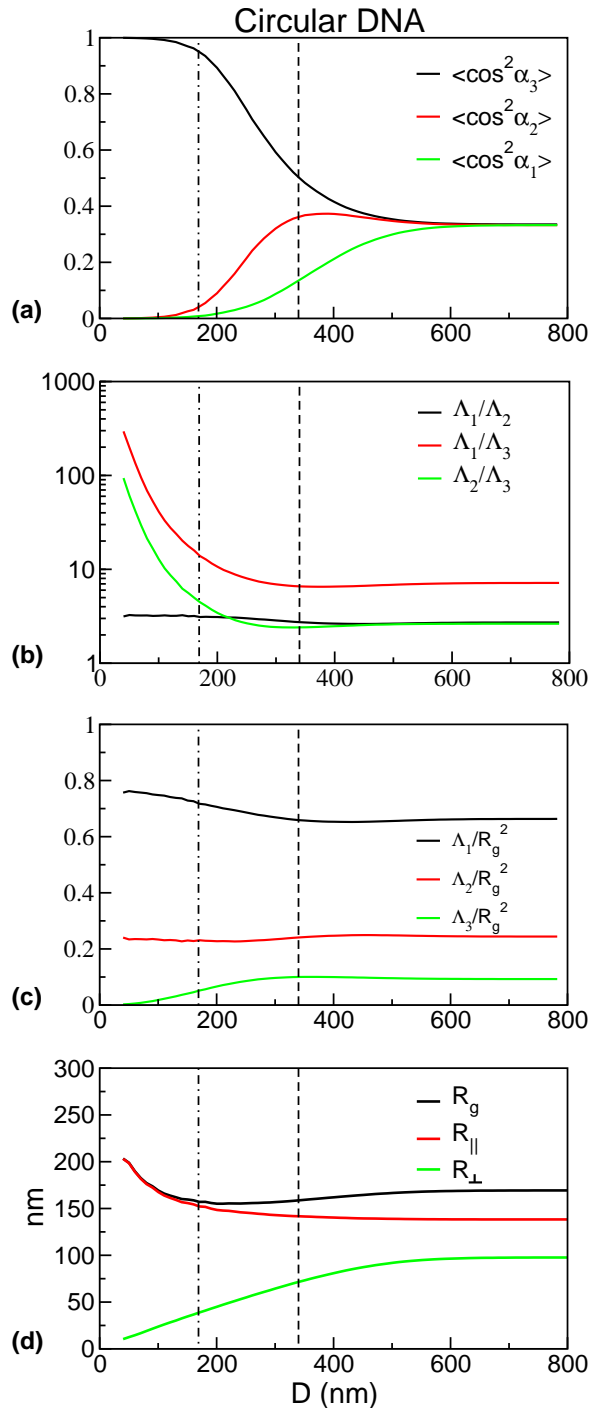


FIG. 5: Metric properties of a circular chain $L_c = 3604$ nm inside a slit of width D . The orientation, shape and size of the gyration ellipsoid of the confined ring are shown in panels (a–c). The root mean square values of the ring radius of gyration, and its in- and out-of-plane projections are shown in panel (d). The range and scale of the x axis (representing the slit width, D) is common to all panels. The two vertical lines mark the reference slit widths R_g^0 (dot-dashed) and $2R_g^0$ (dashed).

The comparison of panels (b) and (c) in the two figures indicates that the shape of closed chains is significantly more spherical than open ones at all levels of confinement. The effect is aptly illustrated by the typical open and closed chains shown in Fig. 1.

Notwithstanding the different shape, it is found that the changes in the ring orientation and size occur for values of the normalized slit width, D/R_g^0 that are similar to the linear case. In particular, the data in panel (a) show that the in-plane orientation of the ring principal axis of gyration sets in for $D \approx 2R_g^0$ while for the second one occurs at $D \approx R_g^0$. Furthermore the average ring size, R_g , shown in panel (d) has a non-monotonic dependence on D and its minimum value (again given by the opposite trends of $R_{||}$ and R_{\perp}) occurs for $D \approx R_g^0$, as for the linear case.

B. Scaling properties and the deGennes regime

Because the bulk metric scaling exponents ν_{2D} and ν_{3D} are the same for open and closed chains, it is expected that the de Gennes scaling regime, originally based on the blob argument for linear chains, ought to hold for circular ones too.

However, the closed character of the rings introduces correlations in the orientation in pairs of bonds at a large chemical (contour) distance that have no analog in linear chains [64, 65]

To clarify the effect we show in Fig. 6 the same observables reported in Fig. 4 to analyze the de Gennes regime for confined linear chains.

Panel (a) shows that, except for the data at the smallest ring contour length, there is a good overlap of the rescaled ring size versus width curves. In particular, for all considered chain lengths the minimum overall ring size is obtained for $D \approx R_g^0$, consistently with the open chain case

For $D < R_g^0$ the mean in-plane size shows a behaviour that is compatible with the de Gennes scaling regime, as illustrated in panel (b). The power-law fit of the asymptotic data in the figure, i.e. $L_c \geq 3604\text{nm}$ and $D/R_g^0 < 1$, yields the scaling exponent -0.26 ± 0.04 . This value is compatible with the -0.276 value predicted by the de Gennes theory, consistently with what found for the linear case.

C. Topological entanglement

1. Knotting probability

The Monte Carlo strategy employed here and in other previous studies provides the means to characterize the occurrence of non-trivial knots in rings that are circularised in equilibrium. The knotting probability of unconstrained rings depends on several lengthscales such as the molecule's persistence length, its contour length

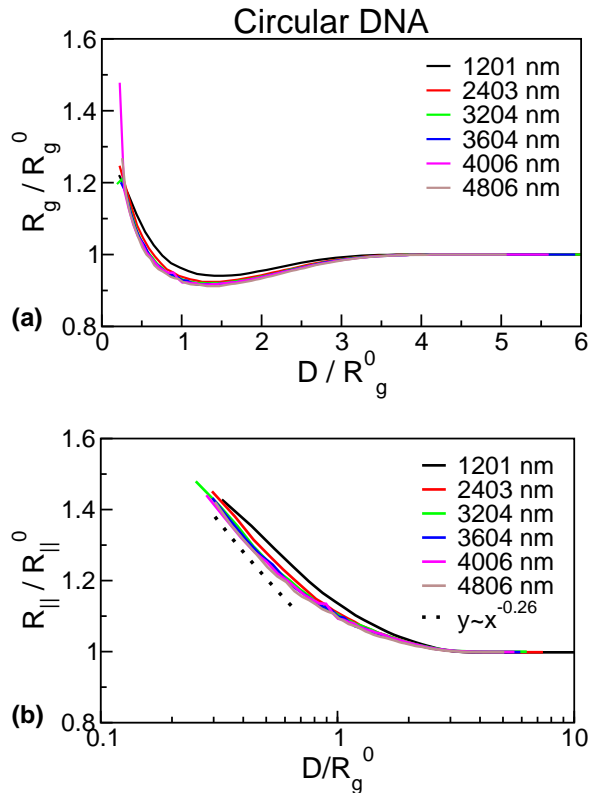


FIG. 6: (a) The minimum three-dimensional size of the ring is achieved when the slit width is about equal to the average radius of gyration of the unconstrained ring. (b) Below such slit width the relationship between the average in-plane size, $R_{||}$, ring contour length, N , and slit width, D , is well accounted for by the de Gennes' blob theory.

and thickness [66, 67]. Accordingly, the topological complexity of the circularised molecules can be tuned, to some extent, by varying these lengths, for example by intervening of the solution ionic strength [43, 68].

Spatial confinement introduces a further lengthscale in the problem, the width of the confining region, which can affect dramatically the molecule's entanglement. The effect has been addressed by several studies of isotropic three-dimensional confinement [17, 23, 25, 45] which established that progressive reduction of the volume resulted in an ever-increasing fraction of knotted molecules and of their geometrical and topological complexity [24].

By comparison, the case of two-dimensional confinement is virtually unexplored, except for lattice polymer models [42, 69, 70]. Making progress in this problem is not only important to fill a conceptual gap but is especially so in view of the dramatic qualitative differences that are expected *a priori* compared to the isotropic, three-dimensional, confinement.

In fact, it should be considered that for extreme two dimensional confinement, i.e. for slit width only slightly larger than the chain intrinsic thickness, over/under-crossings of the chain are impossible and

knots cannot be formed. Therefore, unlike the isotropic case, progressive slit confinement cannot result in an ever increasing complexity of the ring topology and geometry.

To clarify this aspect we investigated the dependence of the knotting probability on D . The results are shown in Fig. 7a and indicate that the ring knotting probability is non-monotonic and for a certain slit width, D_e reaches a maximum enhancement compared to the bulk case. Notice that the peak value exceeds the bulk knotting probability by several factors. The figure indicates that the limiting value of zero knotting probability is rapidly reached for $D < D_e$.

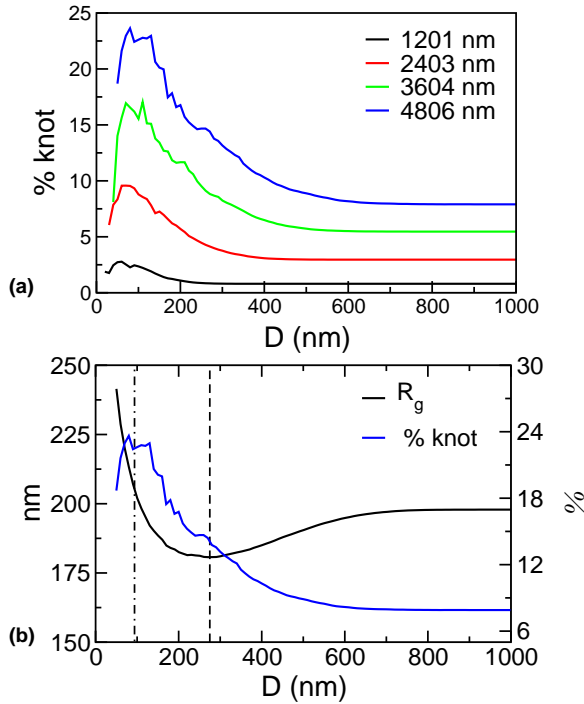


FIG. 7: (a) Knotting probability of equilibrated rings of different contour length. (b) Dependence on the slit width, D , of the average radius of gyration and knotting probability for a circular DNA ring of $L_c = 4806\text{nm}$. The vertical dashed line marks the slit width, D^* , corresponding to the minimum three-dimensional size of the ring. The dot-dashed line marks the maximum of the knotting probability.

It could be intuitively expected that the maximum knotting enhancement occurs for the same slit width, D^* , associated to the maximum chain density (minimum R_g) [42]. This is, however, not the case. In fact, in the example of Fig. 7b the peak of the probability distribution occurs when the slit width is $D_e \approx 90\text{nm}$, which is about one third of D^* . As a matter of fact, over the considered range of contour lengths, D_e is consistently equal to about half the bulk ring size.

2. Knot spectrum

It is most interesting to examine how the various, topologically inequivalent knot types, contribute to the nonmonotonic trend of the overall knotting probability.

The results are shown in Fig. 8a,b which portrays the probability of occurrence of various knot types (including the unknot) for four different slit widths and $L_c = 4.8\mu\text{m}$. It is seen that, at all level of confinement, the knot population consists of very simple knots, and is dominated by the simplest of all, the trefoil or 3_1 knot, whose peak abundance is $\sim 14\%$.

The result is notable in several respects. First, the knot spectrum of Fig. 8a is qualitatively very different from the one of an equivalent model of circular DNA subject to isotropic, spherical confinement [45].

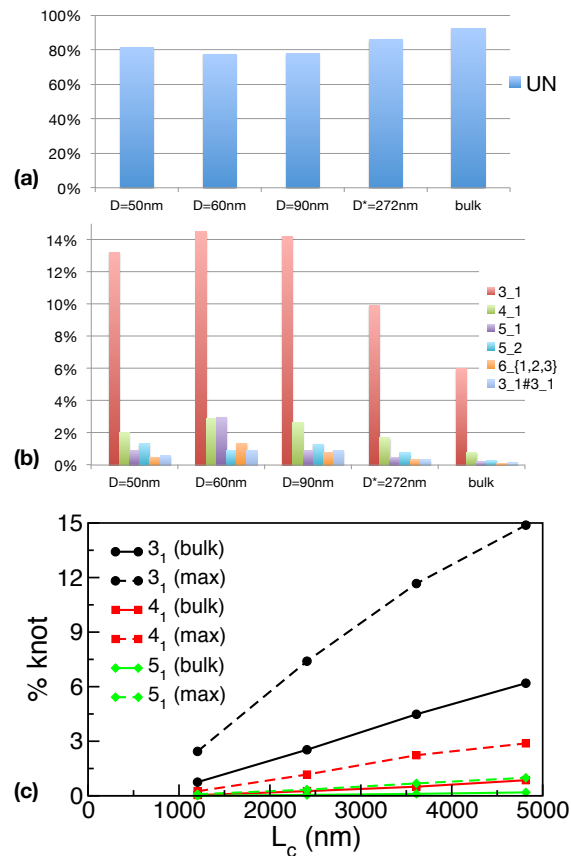


FIG. 8: (a,b) Slit-width dependence of the knot spectrum of confined circular DNA with $L_c = 4806\text{nm}$. D^* is the slit width at which the mean 3D extension of the rings reaches its minimum value. (c) Maximum probability of occurrence for knot types 3_1 , 4_1 and 5_1 as a function of the contour length L_c (dashed curves). Solid curves refer to the corresponding case of unconstrained circular DNAs.

In fact, even for moderate three-dimensional confinement in a sphere of diameter equal to 180nm , the knot spectrum of molecules of $L_c = 3.4\mu\text{m}$ is largely constituted by highly complex knots: trefoils are less than 10 % of the non-trivial knots (which, in turn are 55% of

the ring population). Conversely, for slit confinement, at all considered values of L_c and D , complex knots are virtually absent and the population of simple knot types, such as the trefoil, reaches values that cannot be matched by rings of the same or longer contour lengths subject to any degree of isotropic confinement [23].

We finally turn to the dependence of the peak of the probability of occurrence of simple knots as a function of chain length. The data in Fig. 8c indicate a monotonic increase of the peak probability with L_c . Therefore, the population of simple knots can be further increased compared to the values in panel (b) by suitably confining rings with $L_c > 5\mu\text{m}$. At the same time, it is noticed that the derivative of the peak probability curves decreases with L_c so that, by analogy with the bulk probability case, one can envisage that the curves will eventually decrease for sufficiently large values of L_c . This is an interesting point that would deserve to be addressed in future studies.

3. Knot length

We conclude the topological characterization by reporting on the degree of localization (in space and along the chain) of the knots formed in the confined rings. The knot location along the ring was established using the bottom-up search of the smallest arc(s) that, after closure, has the same topology of the whole ring [57, 71], see the example in Fig. 9.

The average contour length spanned by the knots (all non-trivial topologies) as a function of D is shown in Fig. 10 for rings of length $L_c = 4.8\mu\text{m}$. It is seen that up to the point where the average ring size is minimum, the length of the knotted region is about constant, and drops significantly at smaller slit widths.

The same figure also shows the average in-plane and overall size of the knotted region, which is indicated with R_g^k and $R_{||}^k$, respectively. It is apparent that the drop in knot length occurs when the slit width is about equal to the bulk value of the overall knot size, $D \approx 125\text{nm}$. These results suggest that for knotted polymer rings confined into slits the typical size of the knotted region introduces an additional length scale into the problem that could play a relevant role in understanding the metric and mechanical properties of these confined molecules at equilibrium [70, 72].

V. CONCLUSIONS

The equilibrium properties of linear and circularised model DNA molecules confined in nano-slits were studied by numerical methods. By using thermodynamic reweighting techniques the properties of these systems were systematically profiled as a function of the molecules' contour length and nano-slit width. The analysis proceeded by first considering the molecules'

geometrical properties and next the topological ones. The former included the size, shape and spatial orientation of the molecules in the slit, while the latter consisted of the knotting probability and knot spectrum.

We found that the scaling of the metric properties was described very well by de Gennes' blob theory for both linear and circular molecules of all considered lengths and down to the highest confinement. To the best of our knowledge, it is the first time that the applicability of the blob theory is discussed (and shown to hold) for equilibrated ring polymers. In addition, even for linear molecules, the fact that the de Gennes' scaling is investigated upon varying *both* the molecules' contour length and the slit width represents a significant broadening of the scope of previous investigations. Our results are consistent with the conclusions of recent experiments of nano-slit confinement of linear λ -DNA which found no indications of deviations from de Gennes' blob theory [18].

Finally, and most importantly, we characterized the topological entanglement that is trapped in molecules that circularise in equilibrium inside nano-slits. For both applicative purposes and for fundamental polymer science, the characterization of the physical properties of DNA molecules with various topologies (linear, circular planar, circular knotted) has attracted much interest in the past decades. Our contribution represents a step forward in the characterization of such systems in the presence of confinement: while the three-dimensional confinement has been heavily investigated [23, 25, 26, 28, 45], the two-dimensional one by means of slits is still largely unexplored. Our study has pointed out a remarkable feature that has no parallel with three-dimensional confinement, namely the non-monotonicity of the knotting probability for increasing confinement. Specifically, it is seen that, among the rings resulting from equilibrium circularization (studied without enforcing topology conservation) the fraction of knotted rings has a maximum at a length-dependent slit width, D_e . The peak knotting probability exceeds by several factors the one in the bulk. Upon decreasing D below D_e , the knotting probability decreases very rapidly to zero.

The above result shows that nano-slit confinement ought to be profitably used in contexts where an *a priori* control of the knotted topology of DNA rings is desired. In particular, the non-monotonic dependence of the knotting probability as a function of confinement, makes it possible to conceive experiments where the slit width is tuned so that the knotting probability is either significantly enhanced or largely depressed with respect to the bulk case.

The natural extensions of the present study are twofold. On the one hand it would be interesting to consider much longer chain lengths and establish the detailed length-dependence of D_e and the associated maximum knotting probability. On the other hand, it would be most interesting to repeat the present inves-

tigation to the one-dimensional confinement case (i.e. nano-channels) and analyze how the expected consecutive onsets of the de Gennes and Odijk regimes impact both the geometrical and the topological properties of confined rings.

VI. ACKNOWLEDGEMENTS

We acknowledge support from the Italian Ministry of Education. We thank A. Rosa for useful discussions.

Reprinted with permission from
C. Micheletti and E. Orlandini, *Macromolecules*, 2012,
vol. 45, pp. 8668-8680.
Copyright (2012) American Chemical Society.

-
- [1] J. Han, G. Craighead, *Science* **288**, 1026 (2000).
 [2] K. Jo et al., *Proc. Natl. Acad. Sci. USA* **104**, 2673 (2007).
 [3] M. Zwolak and M. Di Ventra, *Rev. Mod. Phys.* **80**, 141 (2008).
 [4] J. Fu, J. Yoo, J. Han, *Phys. Rev. Lett.* **97**, 018103 (2006).
 [5] R. B. Schoch, J. Han, P. Renaud, *Rev. Mod. Phys.* **80**, 839 (2008).
 [6] B. Maier, J. O. Radler, *Phys. Rev. Lett.* **82**, 1911 (1999).
 [7] F. Drube, K. Alim, G. Witz, G. Dietler, E. Frey, *Nano Lett.* **10**, 1445 (2010).
 [8] D. J. Bonthuis, C. Meyer, D. Stein, C. Dekker, *Phys. Rev. Lett.* **101**, 108303 (2008).
 [9] P.-K. Lin, C.-C. Fu, Y.-L. Chen, Y.-R. Chen, P.-K. Wei, C. H. Kuan, W. S. Fann, *Phys. Rev. E* **76**, 011806 (2007).
 [10] M. Krishnan, I. Monch, P. Schwille, *Nano Lett.* **7**, 170 (2007).
 [11] C. Micheletti, D. Marenduzzo, and E. Orlandini, *Physics Reports* **504**, 1 (2011).
 [12] P.-G. de Gennes, *Scaling concepts in Polymer Physics* (Cornell University Press, Ithaca, New York, 1979).
 [13] T. Odijk, *Phys. Rev. E* **77**, 060901 (2008).
 [14] F. Valle, M. Favre, P. De Los Rios, A. Rosa, G. Dietler, *Phys. Rev. Lett.* **95**, 158105 (2005).
 [15] W. Reisner, K. J. Morton, R. Riehn, Y. M. Wang, Z. Yu, M. Rosen, J. C. Sturm, S. Y. Chou, E. Frey, and R. H. Austin, *Phys. Rev. Lett.* **94**, 196101 (2005).
 [16] E. Ercoloni, F. Valle, J. Adamcik, G. Witz, R. Metzler, P. D. L. Rios, J. Roca, and G. Dietler, *Phys. Rev. Lett.* **98**, 058102 (2007).
 [17] D. Marenduzzo, C. Micheletti, and E. Orlandini, *Journal of Physics: Condensed Matter* **22**, 283102 (2010).
 [18] J. Tang, S. L. Levy, D. W. Trahan, J. J. Jones, H. G. Craighead, and P. S. Doyle, *Macromolecules* **43**, 7368 (2010).
 [19] T. Odijk, *Macromol.* **16**, 1340 (1983).
 [20] Y. Wang, D. Tree, and K. Dorfman, *Macromolecules* **44**, 6594 (2011).
 [21] J. P. J. Michels, F. W. Wiegels, *J. Phys. A: Math. Gen.* **22**, 2393 (1989).
 [22] M. C. Tesi, E. J. Janse Van Rensburg, E. Orlandini, S. G. Whittington, *Topology and geometry in polymer science*, edited by S. G. Whittington, D. W. Sumners and T. Lodge, *IMA Volumes in Mathematics and Its Application* **103**, 135 (1998).
 [23] C. Micheletti, D. Marenduzzo, E. Orlandini, D. W. Sumners, *J. Chem. Phys.* **124**, 064903 (2006).
 [24] L. Tubiana, E. Orlandini, and C. Micheletti, *Phys. Rev. Lett.* **107**, 188302 (2011).
 [25] J. Arsuaga, M. Vázquez, S. Trigueros, D. W. Sumners, J. Roca, *Proc. Natl. Acad. Sci. USA* **99**, 5373 (2002).
 [26] J. Arsuaga, M. Vázquez, P. McGuirk, S. Trigueros, D. W. Sumners, J. Roca, *Proc. Natl. Acad. Sci. USA* **102**, 9165 (2005).
 [27] R. Matthews, A. A. Louis, J. M. Yeomans, *Phys. Rev. Lett.* **102**, 088101 (2009).
 [28] D. Marenduzzo, E. Orlandini, A. Stasiak, D. W. Sumners, L. Tubiana, and C. Micheletti, *Proc Natl Acad Sci U S A* **106**, 22269 (2009).
 [29] W. M. Gelbart and C. M. Knobler, *Science* **323**, 1682 (2009).
 [30] A. Leforestier, A. Siber, F. Livolant, and R. Podgornik, *Biophys J* **100**, 2209 (2011).
 [31] J. Z. Y. Chen and D. E. Sullivan, *Macromolecules* **39**, 7769 (2006).
 [32] D. I. Dimitrov, A. Milchev, K. Binder, L. I. Klushin, and A. M. Skvortsov, *J. Chem. Phys.* **128**, 234902 (2008).
 [33] M. Atapour and C. Soteros and S.G. Whittington, *J. Phys. A: Math. Theor.* **42**, 322002 (2009).
 [34] A. Y. Grosberg, *Phys. Rev. Lett.* **85**, 3858 (2000).
 [35] N. T. Moore, R. C. Lua, A. Y. Grosberg, *Proc. Natl. Acad. Sci. USA* **101**, 13431 (2004).
 [36] J. B. Schvartman, A. Stasiak, *EMBO Rep.* **5**, 256 (2004).
 [37] P. Virnau, A. Mallam, and S. Jackson, *Journal of Physics: Condensed Matter* **23**, 033101 (2011).
 [38] P. Virnau, Y. Kantor, M. Kardar, *J. Am. Chem. Soc.* **127**, 15102 (2005).
 [39] D. W. Sumners, C. Ernst, S. J. Spengler, N. R. Cozzarelli, *Quarterly reviews of biophysics* **28**, 253 (1995).
 [40] Z. Liu, J. K. Mann, E. L. Zechiedrich and H. S. Chan HS, *J. Mol. Biol.* **361**, 268 (2006).
 [41] Z. Liu, L. Zechiedrich, and H. S. Chan, *J Mol Biol* **400**, 963 (2010).
 [42] M. C. Tesi, E. J. Janse Van Rensburg, E. Orlandini, S. G. Whittington, *J. Phys. A: Math. Gen.* **27**, 347 (1994), ISSN 0305-4470.
 [43] V.V. Rybenkov, N. R. Cozzarelli, A. V. Vologodskii, *Proc. Natl. Acad. Sci. USA* **90**, 5307 (1993).
 [44] M. K. Shimamura, T. Deguchi, *Phys. Lett. A* **274**, 184 (2000).
 [45] C. Micheletti, D. Marenduzzo, E. Orlandini, D. W. Sumners, *Biophys J.* **95**, 3591 (2008).
 [46] H. H. Strey, R. Podgornik, D. C. Rau, and V. A. Parsegian, *Curr Opin Struct Biol* **8**, 309 (1998).

- [47] A. Leforestier and F. Livolant, Proc Natl Acad Sci U S A **106**, 9157 (2009).
- [48] A. Grosberg and A. Zhestkov, J. Biomol. Struct. Dyn. **3**, 515 (1985).
- [49] G. C. Rollins, A. S. Petrov, and S. C. Harvey, Biophys J **94**, 38 (2008).
- [50] M. C. Tesi, E. J. Janse Van Rensburg, E. Orlandini, S. G. Whittington, J. Stat. Phys. **82**, 155 (1996).
- [51] P. De Gennes, Isr. J. Chem. **14**, 154 (1975).
- [52] M. Daoud, J. P. Cotton, B. Farnoux, G. Jannink, G. Sarma, H. Benoit, C. Duplessix, C. Picot, and P. G. de Gennes, Macromolecules **8**, 804 (1975).
- [53] N. Clisby, Phys. Rev. Lett. **104**, 055702 (2010).
- [54] E. Orlandini, S. G. Whittington, Rev. Mod. Phys. **79**, 611 (2007).
- [55] W. R. Taylor, Nature **406**, 916 (2000).
- [56] K. Koniaris, M. Muthukumar, Phys. Rev. Lett. **66**, 2211 (1991).
- [57] L. Tubiana, E. Orlandini, and C. Micheletti, Prog. Theor. Phys. **191**, 192 (2011).
- [58] K. Millett, A. Dobay, A. Stasiak, Macromol. **38**, 601 (2005).
- [59] C. Haber, S. A. Ruiz, and D. Wirtz, Proc Natl Acad Sci U S A **97**, 10792 (2000).
- [60] B. Maier and J. O. Rdlr, Macromolecules **34**, 5723 (2001).
- [61] E. Rawdon, A. Dobay, J. C. Kern, K. C. Millett, M. Piatek, P. Plunkett, and A. Stasiak, Macromolecules **41**, 4444 (2008).
- [62] E. J. Rawdon, J. C. Kern, M. Piatek, P. Plunkett, A. Stasiak, and K. C. Millett, Macromolecules **41**, 8281 (2008).
- [63] A. Rosa, E. Orlandini, L. Tubiana, C. Micheletti, Macromol. **44**, 8668 (2011).
- [64] G. Witz, K. Rechendorff, J. Adamcik, G. Dietler, Phys. Rev. Lett. **101**, 148103 (2008).
- [65] G. Witz, K. Rechendorff, J. Adamcik, and G. Dietler, Phys. Rev. Lett. **106**, 248301 (2011).
- [66] M.D. Frank-Kamenetskii, A. V. Lukashin, A. V. Volodskii, A. V., Nature **258**, 398 (1975).
- [67] T. Deguchi, K. Tsurusaki, Phys. Rev. E **55**, 6245 (1997).
- [68] N. M. Toan, C. Micheletti, J. Phys. Condens. Matter **18**, S269 (2006).
- [69] C. Soteris, S. G. Whittington, Israel J. Chem. **31**, 127 (1991).
- [70] E. J. Janse van Rensburg, J. Stat. Mech. p. art. no. P03001 (2007).
- [71] B. Marcone, E. Orlandini, A. L. Stella, F. Zonta, J. Phys. A: Math. Gen. **38**, L15 (2005).
- [72] R. Matthews, A. A. Louis, and J. M. Yeomans, Molecular Phys. **109**, 1289 (2011).

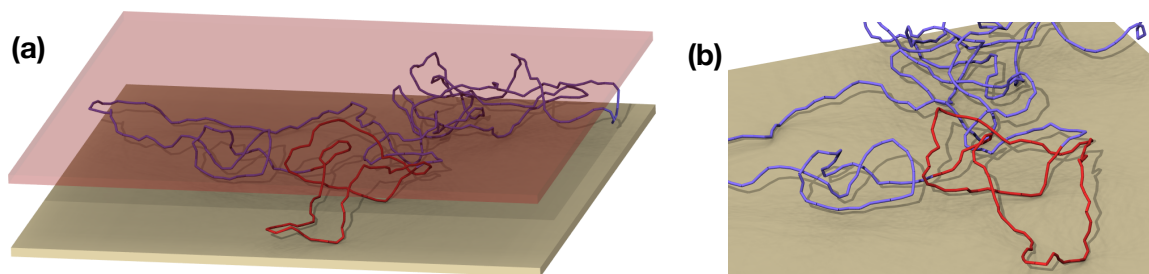


FIG. 9: (a) Trefoil-knotted ring confined in a nanoslit. The configuration is the same as the one shown in Fig. 1c,d. The ring contour length is $0.48 \mu\text{m}$ and the slit width is 70nm . The shortest knotted portion of the ring is highlighted in red. (b) Close-up of the knotted portion; for graphical clarity the slit top is not shown.

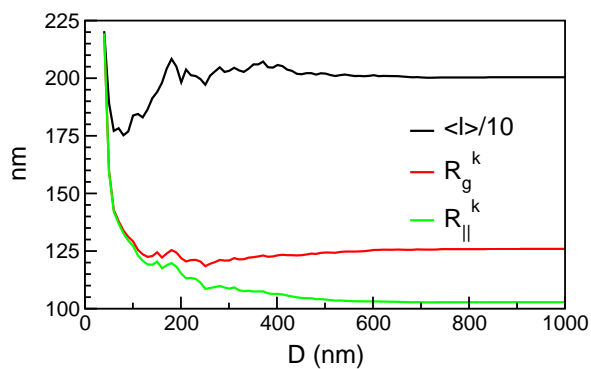


FIG. 10: Three-dimensional and parallel mean extension of the knotted portion of circular trefoil knots with $L_c = 4806\text{nm}$. Circles refer to the average knot size expressed in unit of cylinders.